J. Fluid Mech. (2003), *vol.* 485, *pp.* 171–190.
DOI: 10.1017/S0022112003004415 Printed in the United Kingdom

A note on tidally generated sand waves

By G. BESIO, P. BLONDEAUX AND P. FRISINA

Department of Environmental Engineering, University of Genova,
Via Montallegro 1, 16145 Genova, Italy

(Received 26 June 2002 and in revised form 20 January 2003)

The process leading to the formation of sand waves in tide dominated coastal areas is investigated by means of the linear stability analysis of a flat sandy bottom subject to oscillatory tidal currents. The conditions for the decay or amplification of small bottom perturbations are determined for arbitrary values of the parameters of the problem. According to field observations, the initial growth of sand waves requires a minimum amplitude of the tidal current, even when the critical bed shear stress for the initial motion of sediment is set equal to zero. Moreover the minimum amplitude depends on sediment characteristics. In particular, the analysis shows that sand waves appear only for a sandy bottom and their growth does not take place when a coarse sediment covers the sea bed. The solution procedure extends the truncation method which is often used to describe the flow generated by the interaction of bottom perturbations with the oscillatory tidal current. The obtained results show that the truncation method describes the mechanism inducing the growth of sand waves, but values of the parameters exist for which its results are not quantitatively accurate. Finally, the asymptotic approach for large values of both r, which is the ratio between the amplitude of the horizontal tidal excursion and the wavelength of the bottom perturbations, and of the stress parameter s is modified in the bottom boundary layer to describe cases characterized by values of s of order one, which is the order of magnitude suggested by an analysis of field data.

1. Introduction

Field surveys in tide dominated coastal areas often indicate that the sea bottom is characterized by the presence of bedforms (often called sand waves) with wavelengths of the order of hundreds of metres and amplitudes of the order of a few metres, the crests being almost perpendicular to the direction of the main tidal current.

Finite-amplitude sand waves were investigated by Fredsøe & Deigaard (1992) with an approach similar to that proposed by Fredsøe (1982) for dunes in fluvial environments. The approach describes the form of sand waves, but it is unable to explain the mechanism causing these bedforms and to predict the conditions which lead to their appearance.

As pointed out in other studies of the phenomenon (Hulscher 1996*a*; Gerkema 2000), the process which gives rise to the formation of sand waves, is similar to that causing sea ripples under gravity waves (Sleath 1976; Blondeaux 1990, 2001; Blondeaux & Vittori 1999). In fact, the interaction of the oscillatory tidal flow with bottom perturbations gives rise to a steady streaming in the form of recirculating cells. When the net displacement of the sediment dragged by this steady streaming is directed toward the crests of the bottom waviness, the amplitude of the perturbation grows and bedforms are generated. On the other hand, the flat bottom configuration

turns out to be stable when the net motion of the sediment is directed toward the troughs of the bottom waviness.

First attempts to describe sand wave appearance were made by Hulscher, de Swart & de Vriend (1993) and de Swart & Hulscher (1995) using depth average models with parameterizations of secondary currents in the vertical plane. The first contribution aimed at investigating sand wave formation by means of a fully three-dimensional model is due to Hulscher (1996*a*), who formulated a model based on the three-dimensional shallow-water equations. In Hulscher (1996*a*), turbulent stresses are handled by means of the Boussinesq hypothesis and the eddy viscosity is assumed to be constant in time and over the water depth. A constant eddy viscosity gives rise to an acceptable velocity profile, except in a negligible thin layer close to the wall, only when the no-slip condition at the bottom is replaced by a partial slip condition. Finally, the bottom time development is determined using the sediment continuity equation and a simple sediment transport predictor. The analysis predicts the temporal development of bottom perturbations of small amplitude (strictly infinitesimal) and determines the range of parameters for which the bottom perturbations amplify or decay.

The hydrodynamics of the problem are characterized by the presence of the parameter r, which is the ratio between the amplitude of the horizontal tidal excursion and the wavelength of the bottom perturbations. Under field conditions, r is typically large and, as discussed by Gerkema (2000), the truncation method used by Hulscher (1996*a*) to work out the solution provides a good qualitative description of the phenomenon but the quantitative results are not accurate. By exploiting the fact that the problem gives rise to an equation similar to Orr–Sommerfeld equation where the parameter r replaces the Reynolds number and by taking advantage of the large values assumed by r, Gerkema (2000) solved the problem by using an asymptotic approach similar to that developed for the Orr–Sommerfeld equation for large values of the Reynolds number Re (Lin 1967; Drazin & Reid 1981). In this approach, the fluid perturbation is split into two parts: an inviscid outer solution and viscous boundary layers, located at the wall and possibly at 'critical' levels. Moreover, an analysis of the order of magnitude of the terms of the Orr–Sommerfeld equation shows that the wall layer has a thickness of order $Re^{-1/3}$. In following closely such an approach, Gerkema (2000) assumed that the viscous wall layer has a thickness of order $r^{-1/3}$. However, the latter estimate is suitable when the no-slip condition applies at the wall. Since use is made of the partial slip condition, the turbulent basic velocity distribution is approximated by a profile which does not vanish at the bottom unless the parameter s appearing in the model is much larger than one and the turbulent velocity profile is almost coincident with that characterizing the laminar regime. An analysis of field data and previous works on the subject (Hulscher 1996*a*, *b*) suggest that, in the field, s is of order one. In this case, it can be shown (see § 3.3) that the viscous wall layer turns out to be of order $r^{-1/2}$ rather than $r^{-1/3}$ and critical layers do not exist. Gerkema (2000) solved the problem also with two alternative approaches. The former is an extension of Hulscher's (1996*a*) approach and it is strictly valid only for small values of the parameter r. The latter uses a double series expansion and considers values of r much larger than one, even though it fails when r is very large.

In the present work, the problem has been solved for arbitrary values of r and s using a procedure similar to that employed by Vittori (1989) and Vittori & Blondeaux (1990) in a different context. A Fourier series in time is used to compute the stream-function associated with the flow perturbations and the results show that the number of harmonics necessary to obtain an accurate description of the perturbed flow is

relatively small for moderate values of r, but it increases as the parameter r is increased.

The proposed approach is supported by a comparison of the results with those obtained by means of two perturbation approaches based on the assumptions of small and large values of r. In the latter case, we follow closely Gerkema's (2000) analysis, but we modify it taking into account that, for values of the parameter s of order one, a viscous wall layer of thickness proportional to $r^{-1/2}$ exists.

The rest of the paper is organized as follows. In the following section the problem is formulated and the basic flow generated by tide propagation over a flat bottom is described. In § 3, bottom perturbations are introduced and their time development is determined. The results are presented in § 4 and a comparison with field data is made. In § 5, a discussion of the main merits of the analysis and of its limitations is made. The final section is devoted to the conclusions.

2. Formulation of the problem and the basic flow

The formulation of the problem does not differ from that of previous authors. We consider the flow generated by a tidal wave propagating over a cohesionless bed and investigate the time development of the bottom configuration it induces. To allow an easy comparison between the results of the present analysis and those of previous authors, we use, when possible, the same notation as employed by Gerkema (2000). We consider a two-dimensional turbulent flow and we employ a Boussineq type closure and the 'slip velocity' approach of Engelund (1964). Hence, the hydrodynamics of the problem is described by momentum and continuity equations which read

$$\frac{\partial \boldsymbol{u}}{\partial t} + (\boldsymbol{u}\cdot\nabla)\boldsymbol{u} = -\frac{1}{\rho}\nabla p + A\nabla^2\boldsymbol{u}, \quad \nabla\cdot\boldsymbol{u} = 0, \tag{2.1}$$

where x denotes the horizontal coordinate in the direction of tide propagation, z is the vertical coordinate, $\boldsymbol{u} = (u, w)$ are the horizontal and vertical velocity components averaged over turbulence, respectively, and ∇ is the operator defined by $(\partial/\partial x, \partial/\partial z)$. Moreover, the density ρ and the eddy kinematic viscosity A, which is introduced to model Reynolds stresses, are assumed to be constant in space and time.

A constant eddy-viscosity model provides an approximate but still acceptable description of the flow induced by tide propagation provided the no-slip condition at the bottom is replaced by a partial slip condition

$$\frac{\partial u_{\|}}{\partial n} = \tilde{s}u_{\|} \quad \text{at } z = \eta(x,t), \tag{2.2}$$

where $\partial/\partial n$ denotes the derivative in the direction normal to the bottom, $u_{\|}$ indicates the alongslope velocity component and $z = \eta(x,t)$ describes the bottom profile (Engelund 1970). In (2.2), $\tilde{s}$ is a stress parameter, the value of which should be properly chosen. Moreover, at the bed, the normal velocity component should vanish and at the free surface ($z = H$) the rigid-lid approximation is used.

The morphodynamics of the problem is governed by the sediment continuity equation which simply states that convergence (or divergence) of the sediment flux must be accompanied by a rise (or fall) of the bed profile

$$\frac{\partial \eta}{\partial t} + \frac{\partial Q}{\partial x} = 0, \tag{2.3}$$

where Q denotes the sediment flux per unit width divided by a porosity factor. The problem is closed by a sediment transport predictor. Since the tide period is much

larger than the turn-over time of turbulent eddies, the sediment transport rate can be predicted by formulae proposed for steady currents specified with the actual values of the parameters. Here, the relationship proposed by Meyer-Peter & Müller (1948) has been used

$$Q = 8\frac{\sqrt{(\rho_s/\rho - 1)\, g d^3}}{(1-p)} \left(\left|\theta - \gamma \frac{\partial \eta}{\partial x}\right| - \theta_c\right)^{3/2} \left(\theta - \gamma \frac{\partial \eta}{\partial x}\right) \left|\theta - \gamma \frac{\partial \eta}{\partial x}\right|^{-1}, \tag{2.4}$$

where ρ_s, p and d are the density, the porosity and the size of the sediment, respectively, and θ is the dimensionless Shields parameter defined by

$$\theta = \frac{\tau}{(\rho_s - \rho)\, g d}. \tag{2.5}$$

Moreover, τ is the bed shear stress, which can be evaluated easily using the constitutive law and the knowledge of the kinematic eddy viscosity, and θ_c is the critical value of θ for the initial motion of sediment. The term $\gamma \partial \eta/\partial x$ has been added in (2.4), as suggested by Fredsøe (1974), to take into account the bed slope effects. Of course (2.4) is used when $|\theta - \gamma \partial \eta/\partial x|$ is larger than θ_c; otherwise Q vanishes.

In order to model the flow locally induced by the propagation of the tidal wave, we consider the flow over a flat bottom forced by an oscillatory horizontal pressure gradient of angular frequency σ and amplitude P_{0x} which can be related to the amplitude U_m of the depth average velocity oscillations induced by the tidal wave.

The vertical velocity component of the basic flow vanishes identically, while the horizontal component (u_b) can be easily obtained:

$$u_b = \frac{P_{0x}}{2\mathrm{i}\rho\sigma}[1 + \tilde{c}(E^2 \exp(-(1+\mathrm{i})(z/\Delta)) + \exp((1+\mathrm{i})(z/\Delta)))] \exp \mathrm{i}\sigma t + \text{c.c.} \tag{2.6}$$

where Δ is a viscous length defined in terms of the kinematic eddy viscosity A and of the angular frequency of the tide oscillations σ:

$$\Delta = \sqrt{2A/\sigma}, \tag{2.7}$$

and

$$E = \exp((1+\mathrm{i})(H/\Delta)), \quad \tilde{c} = -\frac{\tilde{s}\Delta}{\tilde{s}\Delta(E^2+1) + (1+\mathrm{i})(E^2-1)}. \tag{2.8}$$

As discussed by Gerkema (2000), for moderate values of the parameter $\mu = H^2/(A/\sigma)$, which is the square of the ratio between the water depth and the viscous length, the basic flow can also be approximated as follows:

$$u_b = \tfrac{1}{2} U_0 \left(z_c + \frac{z}{H}\right)\left(2 + z_c - \frac{z}{H}\right) \exp(\mathrm{i}\varphi) \exp(\mathrm{i}\sigma t) + \text{c.c.}, \tag{2.9}$$

where z_c is a dimensionless constant defined in the form

$$z_c = -1 + \sqrt{1 + 2/(\tilde{s}H)}, \tag{2.10}$$

and U_0 and φ are fitting parameters which can be determined by comparing the depth-averaged values of u_b obtained from (2.9) and the exact solution (2.6). In particular, it turns out that

$$U_0 = \frac{U_m}{\left[\frac{2}{3} + z_c\,(2 + z_c)\right]}, \tag{2.11}$$

where U_m is the amplitude of the depth-averaged velocity oscillations induced by the tide.

3. The time development of bottom perturbations

To investigate the stability of the flat bottom configuration, we consider bottom perturbations of small amplitude (strictly infinitesimal) and linearize the problem. A generic component of the bottom perturbation of the form

$$\eta(x,t) = \Pi(t)\cos(kx) = \tfrac{1}{2}\Pi(t)\exp(\mathrm{i}kx) + \text{c.c.} \tag{3.1}$$

can be considered.

In (3.1), Π is assumed to be much smaller than H and k is the perturbation wavenumber.

In order to solve the mathematical problem, it is convenient to introduce dimensionless variables denoted by an apex. The inverse of the wavenumber k^{-1} and the water depth H are used as horizontal and vertical length scales, respectively, U_0 and σ^{-1} are used as velocity and time scales and the quantity $\sqrt{(\rho_s/\rho - 1)\,gd^3}$ scales the sediment transport rate. Finally the dimensionless morphodynamic time scale T' is also introduced $T' = t\sqrt{(\rho_s/\rho - 1)\,gd^3}/[(1-p)H^2]$.

For convenience, in the following, the apex is dropped.

Using the dimensionless variables and taking into account that the streamfunction ψ, such that $u = \partial\psi/\partial z$ and $w = -\delta\partial\psi/\partial x$, can be written in the form

$$\psi(x,z,t) = \Pi(T)\Psi(z,t)\exp(\mathrm{i}x) + \text{c.c.} \tag{3.2}$$

the hydrodynamic problem is posed by the following Orr–Sommerfeld-like equation:

$$\frac{1}{r}\frac{\partial}{\partial t}(N^2\Psi) + \mathrm{i}u_b N^2\Psi - \mathrm{i}\Psi\frac{\partial^2 u_b}{\partial z^2} = \frac{1}{\mu r}N^4\Psi, \tag{3.3}$$

with the following boundary conditions

$$\Psi + \tfrac{1}{2}\mathrm{i}u_b = 0, \quad \frac{\partial^2\Psi}{\partial z^2} + \frac{1}{2}\frac{\partial^2 u_b}{\partial z^2} = s\left(\frac{\partial\Psi}{\partial z} + \frac{1}{2}\frac{\partial u_b}{\partial z}\right) \quad \text{at } z = 0, \tag{3.4}$$

$$\Psi = 0, \quad \frac{\partial^2\Psi}{\partial z^2} = 0 \quad \text{at } z = 1. \tag{3.5}$$

Because the morphodynamic time scale turns out to be much larger than the hydrodynamic scale, the time derivative of Π has consequently been neglected in (3.3). Moreover, in (3.3), the operator N^2 is defined by $N^2 = \partial^2/\partial z^2 - \delta^2$.

Finally, the time development of the bottom configuration is described by

$$\frac{\mathrm{d}\Pi}{\mathrm{d}T} + 2\delta\mathrm{i}\langle\mathcal{Q}\rangle\Pi = 0, \tag{3.6}$$

$$\mathcal{Q} = 12\left[\left|\frac{\delta\Psi_d}{\mu r}\frac{\partial u_b}{\partial z}\right|_{z=0} - \theta_c\right]^{1/2}\left[\frac{\delta\Psi_d}{\mu r}\left(\frac{1}{2}\frac{\partial^2 u_b}{\partial z^2} + \frac{\partial^2\Psi}{\partial z^2} + \delta^2\Psi\right)_{z=0} - \tfrac{1}{2}\mathrm{i}\gamma\delta\right], \tag{3.7}$$

where the $\langle\rangle$ brackets denote the time average over the tide cycle and the small oscillations of the bottom profile, which take place around its average value during the tide cycle, have been neglected.

The problem is characterized by the following dimensionless parameters

$$\delta = kH, \quad r = kU_0/\sigma, \quad \mu = H^2\sigma/A, \quad s = \tilde{s}H, \quad \Psi_d = U_0^2/\left[(\rho_s/\rho - 1)\,gd\right], \quad \gamma. \tag{3.8}$$

At this stage, it may be useful to discuss the typical values of the parameters δ, r, μ, s, Ψ_d and γ for field conditions. The parameter δ is the dimensionless wavenumber of the bottom perturbation. Since sand waves are characterized by wavelengths of the order of hundreds of metres and the water depth is tens of metres, δ assumes values of order one. Typical values of U_m range about 1 ms^{-1} and σ is equal to 1.5×10^{-4} s^{-1} for a semi-diurnal tide and to 7 10^{-5} s^{-1} for a diurnal tide. Therefore, r attains values ranging from 10 to 10^2. Since, as already pointed out, tidal currents are characterized by a time scale much larger than that of the turbulent eddies, an estimate of the eddy viscosity A and of the stress parameter $\tilde{s}$ can be obtained from our knowledge of turbulence structure and eddy viscosity in steady currents and by following the procedure suggested by Hulscher & van den Brink (2001), i.e. by equating A to the depth-averaged value of empirical relationships proposed to describe the kinematic eddy viscosity and forcing the shear stress acting on the bed to be equal to $\rho\,(U_m/C)^2$ where C is a conductance coefficient which depends on the bottom roughness. Using a parabolic profile to describe the z-variations of the kinematic eddy viscosity and the values of C suggested in the literature (see Fredsøe & Deigaard 1992), it turns out that

$$A = \frac{\kappa U_m H}{6C}, \quad \tilde{s} = \frac{6}{H(\kappa C - 2)} \quad \text{with} \quad C = 2.5 \ln\left(\frac{H}{\epsilon}\right) + 6, \tag{3.9a, b}$$

where $\kappa = 0.41$ is the von Kármán's constant, U_m is the depth-averaged velocity and ϵ is the bottom roughness. Similar relationships are obtained using different eddy viscosity profiles even if significant quantitative differences are present. On the basis of these results, it can be concluded that A ranges around 10^{-2}–10^{-1} $\mathrm{m}^2\,\mathrm{s}^{-1}$ and $\tilde{s}$ around 10^{-2}–10^{-1} m^{-1}. It follows that typical values of μ and s are of order 1. Indeed, figures 5 and 6 of Hulscher (1996*b*) show that average conditions of the North Sea are characterized by values of s ($s = \hat{S}/E_v$) smaller than 1 while in the Middelkerke bank, s can be larger than 1 but it is smaller than 2. The sediment mobility number Ψ_d ranges between order 10^2 for fine sand and strong currents and order 1 for coarse sand and weak currents. Finally, γ is the dimensionless bed-slope parameter which typically assumes values of order one. In particular, Fredsøe (1974) used $\gamma = 0.1$.

Since the morphodynamic time scale is much larger than the hydrodynamic time scale (the tide period), the problem posed by (3.3)–(3.6) has been split into two parts: the hydrodynamics governed by equations (3.3)–(3.5), the solution of which provides Ψ, and the morphodynamics governed by (3.6), the solution of which provides the time behaviour of Π.

The hydrodynamics have been solved here following an approach which holds for arbitrary values of r and is based on a procedure similar to that employed by Vittori (1989) and Vittori & Blondeaux (1990) in a different context.

To test the present approach, results have been obtained for both small and large values of r, the other parameters being fixed, and they have been compared with those derived by means of perturbation approaches based on the assumptions $r \ll 1$ and $r \gg 1$, respectively.

3.1. *The hydrodynamic problem for arbitrary values of r*

Since the basic flow is time periodic, the function Ψ can be expanded as a Fourier series in time

$$\Psi = \sum_{n=-\infty}^{\infty} \hat{\Psi}_n(z) \mathrm{e}^{\mathrm{i}nt}. \tag{3.10}$$

Then, substitution of (3.10) into (3.3) and (3.6) leads to the following system of coupled linear ordinary differential equations

$$\frac{\mathrm{i}n}{r}N^2\hat{\Psi}_n+\mathrm{i}\left[\hat{U}N^2\hat{\Psi}_{n-1}+\hat{U}^*N^2\hat{\Psi}_{n+1}\right]-\mathrm{i}\left[\frac{\mathrm{d}^2\hat{U}}{\mathrm{d}z^2}\hat{\Psi}_{n-1}+\frac{\mathrm{d}^2\hat{U}^*}{\mathrm{d}z^2}\hat{\Psi}_{n+1}\right]=\frac{1}{\mu r}N^4\hat{\Psi}_n, \quad (3.11)$$

along with the following boundary conditions

$$\hat{\Psi}_n=0, \quad \frac{\mathrm{d}^2\hat{\Psi}_n}{\mathrm{d}z^2}=0 \quad \text{at } z=1, \quad (3.12)$$

$$(\hat{\Psi}_n,\hat{\Psi}_1,\hat{\Psi}_{-1})=\left(0,-\frac{\hat{U}}{2},-\frac{\hat{U}^*}{2}\right) \quad \text{at } z=0, \quad (3.13)$$

$$\left(\frac{\mathrm{d}^2}{\mathrm{d}z^2}-s\frac{\mathrm{d}}{\mathrm{d}z}\right)(\hat{\Psi}_n,\hat{\Psi}_1,\hat{\Psi}_{-1})=\left(-\frac{1}{2}\frac{\mathrm{d}^2}{\mathrm{d}z^2}+s\frac{\mathrm{d}}{\mathrm{d}z}\right)(0,\hat{U},\hat{U}^*) \quad \text{at } z=0. \quad (3.14)$$

In (3.11)–(3.14), the basic flow u_b has been written in the form

$$u_b=\hat{U}(z)\mathrm{e}^{\mathrm{i}t}+\hat{U}^*(z)\mathrm{e}^{-\mathrm{i}t}. \quad (3.15)$$

Neglecting harmonics higher than the $\mathcal{N}$th in the Fourier series (3.10), the functions $\hat{\Psi}_n$ can be determined numerically using a second-order Runge–Kutta scheme and a shooting procedure. More precisely, starting from $z=1$, a set of $2\mathcal{N}+1$ linearly independent solutions $\hat{\Psi}_n^{(j)}$ are obtained assuming linearly independent values for the first and third derivatives of $\hat{\Psi}_n$. Then, the solution is determined as a linear combination of $\hat{\Psi}_n^{(j)}$ which satisfies the boundary conditions at the bottom. The number $\mathcal{N}$ of harmonics retained in (3.10) has been chosen on the basis of numerical experiments. More details on the procedure can be found in Vittori (1989).

3.2. *The hydrodynamic problem for $r \ll 1$*

Although unrealistic in practical situations, the case $r \ll 1$ is the easiest to analyse and provides results which can be used to test the procedure outlined in the previous section.

When $r \ll 1$, the stream function Ψ can be expanded in the form

$$\Psi=\Psi_0^{(0)}+r\Psi_1^{(0)}+\text{h.o.t.} \quad (3.16)$$

where the index (0) indicates contributions determined in the limit $r \to 0$.

Then, the problems obtained at order r^0 and r^1, by substitution of (3.16) into (3.3)–(3.4), can be solved assuming

$$\Psi_0^{(0)}=\hat{\Psi}_{0,1}^{(0)}\mathrm{e}^{\mathrm{i}t}+\text{c.c.}, \quad \Psi_1^{(0)}=\hat{\Psi}_{1,0}^{(0)}+\hat{\Psi}_{1,2}^{(0)}\mathrm{e}^{2\mathrm{i}t}-\text{c.c.} \quad (3.17)$$

The determination of $\hat{\Psi}_{i,j}$ is straightforward. For example, it can be easily verified that $\hat{\Psi}_{0,1}^{(0)}$ reads

$$\hat{\Psi}_{0,1}^{(0)}=c_1^{(0)}\exp(\delta z)+c_2^{(0)}\exp(-\delta z)+c_3^{(0)}\exp\left(z\sqrt{\delta^2+\mathrm{i}\mu}\right)+c_4^{(0)}\exp\left(-z\sqrt{\delta^2+\mathrm{i}\mu}\right). \quad (3.18)$$

Further details are omitted and the results are directly presented in the following.

3.3. *The hydrodynamic problem for $r \gg 1$*

Since in (3.3) the small parameter r^{-1} multiplies the highest derivative, for large values of r, the flow domain can be split into an inviscid core region, where z is of order one, and a viscous boundary layer close to the bottom.

For the purpose of finding $\Psi^{(\infty)}$, hereinafter the index (∞) indicates contributions determined assuming values of r much larger than one, the basic velocity can be approximated by the much simpler profile (2.9), which provides a good approximation when μ is of order 1. Then the solution can be written in the form

$$\Psi^{(\infty)} = c_1^{(\infty)}\phi_1 + c_2^{(\infty)}\phi_2, \tag{3.19}$$

where the functions ϕ_1 and ϕ_2 are given in Gerkema (2000). The forcing of the boundary conditions at the free surface allow us to find a relationship between the constants $c_1^{(\infty)}$ and $c_2^{(\infty)}$, but not to determine both of them. In fact, it can be verified that the two boundary conditions at the free surface are equivalent because of the momentum equation.

The inviscid balance should be corrected near the bottom, where a boundary layer develops and viscous effects turn out to be relevant. In the classical Orr–Sommerfeld equation, the thickness of this viscous layer is proportional to the $(-1/3)$-power of the Reynolds number (if $Re \gg 1$), because the basic velocity profile vanishes at the wall. However, in the present case, the basic flow described by (2.9) remains finite at the bottom and an analysis of the order of magnitude of the different terms appearing in (3.3) suggests that the thickness of the bottom boundary layer is of $O(r^{-1/2})$.

Hence the analysis requires the introduction of the variable ξ defined as follows

$$\xi = r^{1/2}z. \tag{3.20}$$

Then the basic flow and the streamfunction associated with the perturbation should be expanded in the form

$$u_b = u_{b0} + r^{-1/2}u_{b1} + r^{-1}u_{b2} + \text{h.o.t.} \tag{3.21}$$

$$\Psi = \Psi_0^{(\infty)} + r^{-1/2}\Psi_1^{(\infty)} + r^{-1}\Psi_2^{(\infty)} + \text{h.o.t.} \tag{3.22}$$

By substituting (3.21) and (3.22) into (3.3) and (3.6) and equating likewise powers of $r^{-1/2}$, the functions $\Psi_i^{(\infty)}$ can be determined. It turns out that

$$\Psi_0^{(\infty)} = -\tfrac{1}{2}z_c(2+z_c)\cos(t+\varphi), \quad \Psi_1^{(\infty)} = c_3^{(\infty)}\xi, \tag{3.23}$$

$$\Psi_2^{(\infty)} = -\frac{c_4^{(\infty)}}{\mathrm{i}\mu u_b(t)}\exp\left(-\sqrt{\mathrm{i}\mu u_b(t)}\xi\right) + c_5^{(\infty)}\xi + c_6^{(\infty)},$$

where $c_3^{(\infty)}$, $c_4^{(\infty)}$, $c_5^{(\infty)}$ and $c_6^{(\infty)}$ are constants to be determined. Matching $\Psi_0^{(\infty)}$ with the inviscid solution determines the value of $c_2^{(\infty)}$ while matching $\Psi_1^{(\infty)}$ determines the value of $c_3^{(\infty)}$. The constants $c_j^{(\infty)}$ $(j = 4, 5, 6)$ are determined by the matching at the next order of approximation which requires the evaluation of further terms of the streamfunction in the inviscid region. The first two terms of (3.22) correspond to the largest terms of the outer solution written using the inner variable and strong gradients of Ψ appear only considering $\Psi_2^{(\infty)}$.

As already discussed by Gerkema (2000), the whole procedure breaks down when the flow reverses, i.e. when the basic velocity profile u_b vanishes in the whole water column. The problem can be easily circumvented. Indeed during the time intervals for which u_b is close to zero, the sediment flow rate vanishes and there are no significant morphodynamic implications.

3.4. *The morphodynamic problem*

Once the streamfunction associated with the bottom perturbation is computed, the temporal development of the amplitude Π of the generic component of the perturbation can be evaluated from (3.6)

$$\Pi = \Pi_0 \ \exp\{\Gamma T\} = \Pi_0 \ \exp\left\{\left\langle -24\left[\left|\frac{\delta\Psi_d}{\mu r}\frac{\partial u_b}{\partial z}\right|_{z=0} - \theta_c\right]^{1/2} \times\left[\mathrm{i}\frac{\delta^2\Psi_d}{\mu r}\left(\frac{1}{2}\frac{\partial^2 u_b}{\partial z^2} + \frac{\partial^2\Psi}{\partial z^2} + \delta^2\Psi\right)_{z=0} + \tfrac{1}{2}\gamma\delta^2\right]\right\rangle T\right\}. \tag{3.24}$$

4. The results

Before discussing the results on the morphodynamic stability, obtained on the basis of the procedure outlined in §§ 3.1 and 3.4, we compare the streamfunction and other relevant quantities valid for arbitrary values of r with the results of the asymptotic analyses for values of r much smaller or much larger than one. This has been done to test the implementation of the numerical algorithm and to ascertain the reliability of the results. Because the asymptotic solution for large values of r is based on the approximate basic velocity profile, use is made of (2.9). In figure 1 the function $\Psi(z)$ computed by means of (3.10) is compared with that found for r tending to zero, when the values of δ, μ and s are fixed and r is decreased ($r = 10, 1, 0.1$). As r tends to become small, the expansion (3.10) provides results close to those obtained on the basis of the asymptotic analysis described in § 3.2 and for r equal to 0.1 the two solutions are practically indistinguishable. Of course, for small values of r the streamfunction is dominated by the first term in (3.16) and by the harmonics $\mathrm{e}^{\mathrm{i}t}$ and $\mathrm{e}^{-\mathrm{i}t}$ in (3.10). For an exhaustive comparison, we have not only compared $\hat{\Psi}_1$ with $\Psi_{0,1}^{(0)}$, but also $\hat{\Psi}_0$ and $\hat{\Psi}_2$ divided by r with $\Psi_{1,0}^{(0)}$ and $\Psi_{1,2}^{(0)}$, respectively.

A comparison is also made between (3.10) and the asymptotic solution for large values of r. In figure 2 the streamfunction is plotted for fixed values of δ, μ and s and increasing values of r at particular phases of the cycle. As expected, for increasing values of r, the agreement between (3.19) and (3.10) improves and for large values of r the two approaches provide coincident results and in particular the function Ψ becomes real as predicted by the asymptotic analysis for large values of r. Hence (3.24) shows that the real part Γ_r of Γ is always negative since it turns out to be equal to

$$\left\langle -12\left[\left|\frac{\delta\Psi_d}{\mu r}\frac{\partial u_b}{\partial z}\right|_{z=0} - \theta_c\right]^{1/2}\gamma\delta^2\right\rangle,$$

i.e. the stabilizing part related to the bed slope. Therefore for large values of r, the other parameters being fixed, no growth of the bottom perturbations takes place and the flat bottom configuration turns out always to be stable.

Once the reliability of the procedure is ascertained, the stability of the flat bottom configuration can be investigated by evaluating the growth rate Γ for different values of the parameters. Since the approach described in § 3.1 does not require approximation of the basic flow by (2.9), in the following the results have been obtained making use of the full solution. Both the real Γ_r and the imaginary Γ_i parts of Γ are computed. While the real part of Γ is related to the growth or decay of the

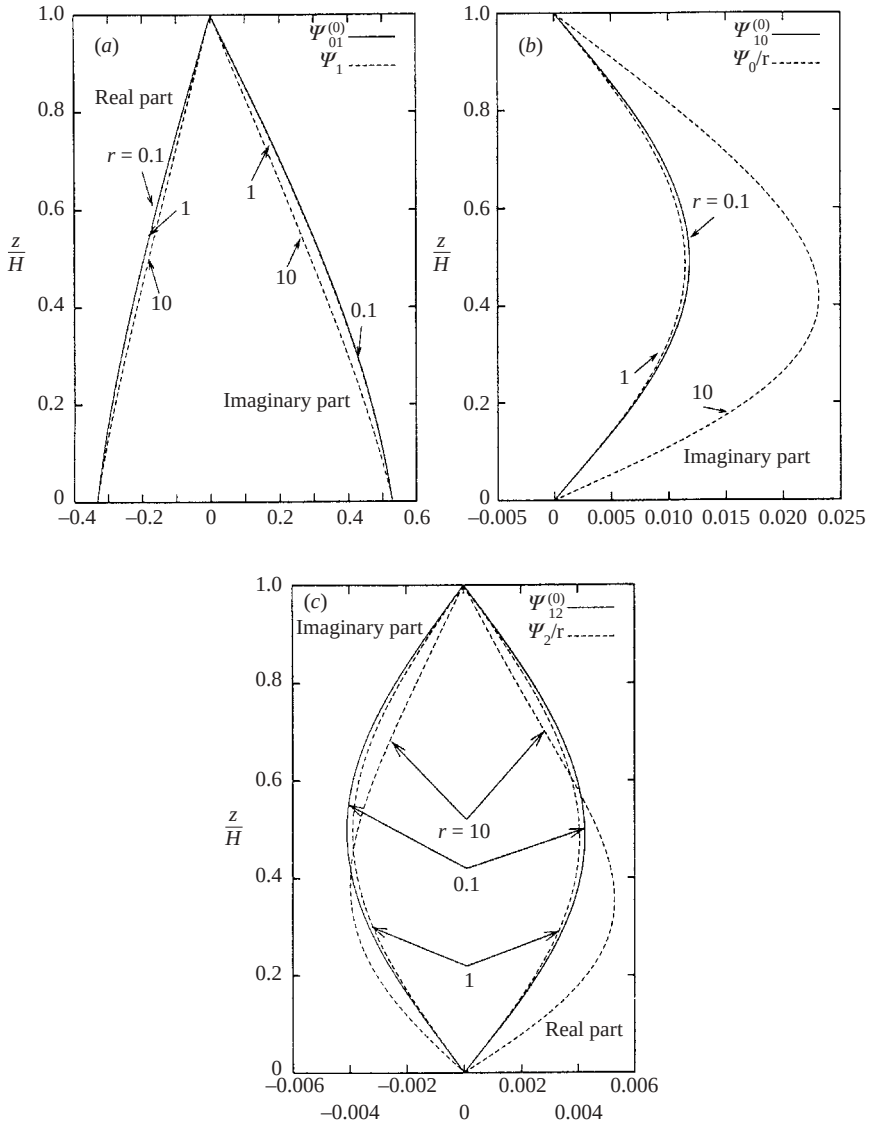

FIGURE 1. Harmonic components of the streamfunction perturbation induced by a bottom waviness. Comparison between the exact solution and the asymptotic solution for small values of r. (*a*) $\hat{\Psi}_1$ and $\Psi_{0,1}^{(0)}$; (*b*) $(\hat{\Psi}_0/r)$ and $\Psi_{1,0}^{(0)}$ (both $\hat{\Psi}_0$ and $\Psi_{1,0}^{(0)}$ are imaginary); (*c*) $(\hat{\Psi}_2/r)$ and $\Psi_{1,2}^{(0)}$. ($\mu = 1$, $s = 0.8$, $\delta = 0.35$).

amplitude of the bottom perturbations, their migration speed is controlled by the imaginary part of Γ. Because of the symmetry of the problem, no migration of the bottom forms is expected to take place after a tide cycle and indeed Γ_i vanishes for whatever set of the parameters is considered.

In order to allow predictions of the most unstable component of the bed perturbation, it is convenient to replace r by the new parameter $\hat{r}$

$$\hat{r} = \frac{U_0}{\sigma H}, \tag{4.1}$$

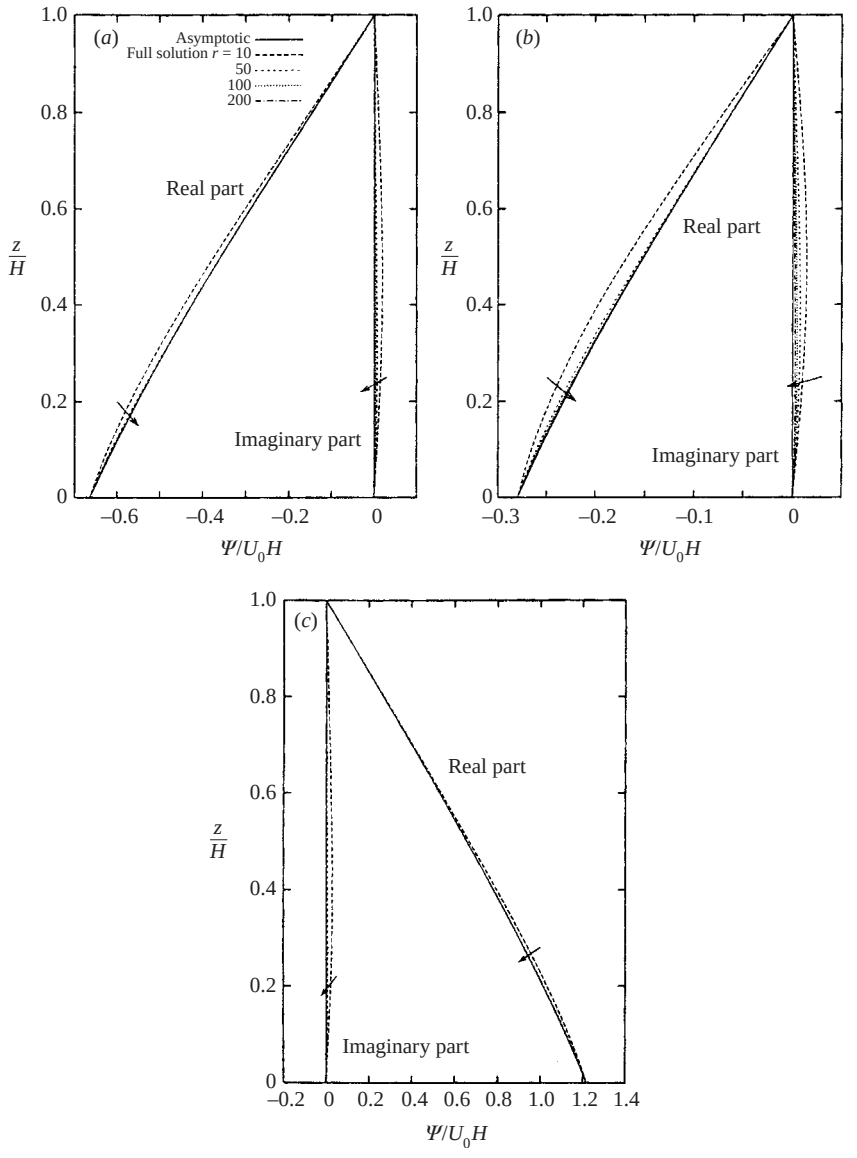

FIGURE 2. Streamfunction Ψ at different phases of the cycle. Comparison between the exact solution and the asymptotic solution for large values of r which turns out to be real. ($\mu = 1$, $s = 0.8$, $\delta = 0.25$, $\mathcal{N} = 150$). (*a*) $t = 0$, (*b*) $t = 3\pi/4$, (*c*) $t = 5\pi/4$.

which does not depend on the characteristics of the bottom perturbations. Notice also that $r = \hat{r}\delta$. Moreover, in the literature (see Belderson, Johnson & Kenyon 1982) the presence of sand waves in a particular site, where the water depth and the bottom roughness are fixed, is related to the strength of the tidal current. To discuss the appearance of sand waves in terms of just one parameter containing U_0, it is convenient to introduce the new viscous parameter

$$\hat{\mu} = \frac{U_0 H}{A}. \tag{4.2}$$

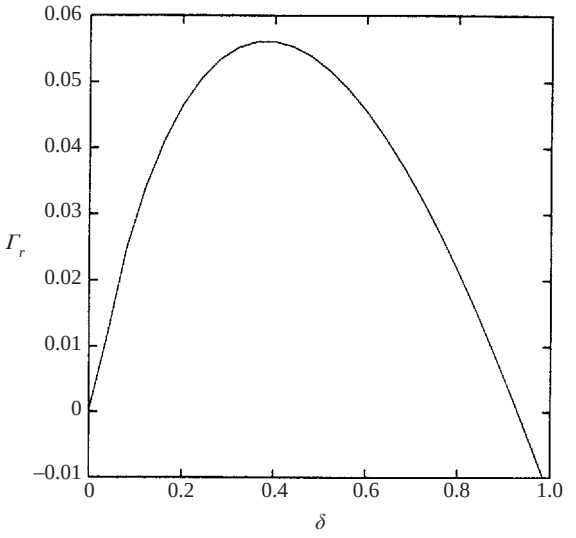

FIGURE 3. Dimensionless growth rate Γ_r *vs.* the dimensionless wavenumber δ of the bottom perturbation. Model parameters are: $\hat{\mu} = 112.5$, $s = 1.02$, $\hat{r} = 79$, $\hat{\Psi}_d = 0.0045$, $\gamma = 0.05$ and $\theta_c = 0.047$.

In fact, (3.9a, b) show that A is proportional to U_0. Then, $\hat{\mu}$ is independent of U_0 and depends only on the relative roughness size. Similarly, it is convenient to define the new sediment parameter

$$\hat{\Psi}_d = \frac{(H\sigma)^2}{(\rho_s/\rho - 1)\, gd}. \tag{4.3}$$

It turns out that $\hat{\mu} = \mu\hat{r}$ and $\hat{\Psi}_d = \Psi_d/\hat{r}^2$.

The performances of the model can be evaluated by looking at figures 3 and 4. Figure 3 shows the amplification rate Γ_r for $\hat{\mu} = 112.5$, $s = 1.02$, $\hat{r} = 79$, $\hat{\Psi}_d = 0.0045$ and $\gamma = 0.05$, values of the parameters which are chosen to reproduce the site SW1 located in the North Sea at 51°35′N and 3°2′E where sand waves have been observed (see figure 4 where the bottom topography is plotted) and tidal currents were measured. The bottom roughness has been evaluated assuming that wave ripples were present, characterized by a wavelength l of about 20 cm. Their height Δ_r is assumed to be $0.17l$ (Sleath 1984) and the bottom roughness is fixed equal to $3\Delta_r$ as suggested by Van Rijn (1981). If it is assumed that actual sand waves are generated by the growth of the bottom perturbations characterized by the largest amplification rate and it is taken into account that Γ_r is maximum for $\delta = \delta_{max} = 0.4$ and the local water depth is about 21 m, the model predicts the formation of sand waves characterized by a wavelength equal to about 315 m, a value close to the observed wavelengths ranging between 165 m and 255 m (see figure 4).

The data of figure 4 and the relationships (3.9a, b) show that field cases are characterized by a value of $\hat{\mu}$ of order 100 while s depends on the relative bottom roughness and falls in a small range around 1. Fixing $\hat{\mu} = 112.5$ and $s = 1.02$, it is interesting to look at model predictions for a fine sandy bottom ($\Psi_d = 0.0045$) and varying the parameter $\hat{r}$ which, in a particular site, is proportional to the current strength U_0. The results are shown in figure 5 where Γ_r is plotted versus δ. For small values of $\hat{r}$, sediment transport does not take place and the bottom configuration does

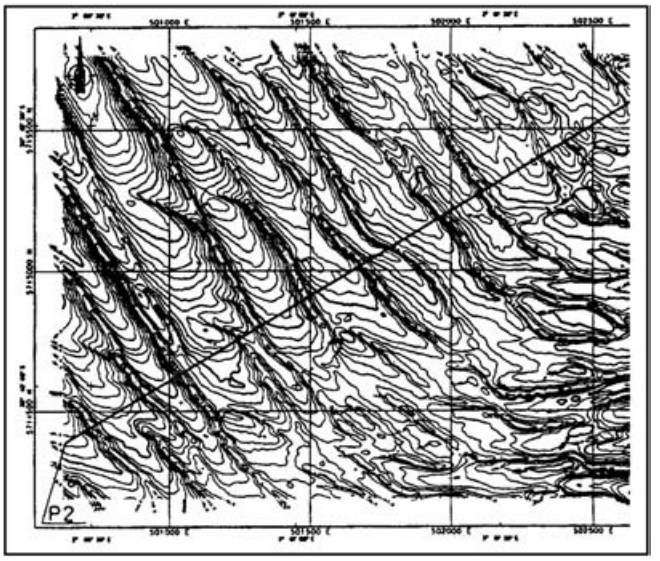

FIGURE 4. Sand waves data. Contour map of the seabed at 51° 35′ N and 3° 2′ E measured in 1988 (grid size = 500 m).

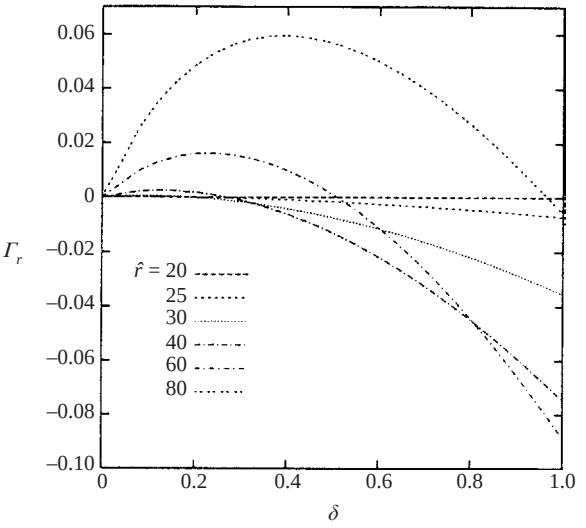

FIGURE 5. Dimensionless growth rate Γ_r *vs.* the dimensionless wavenumber δ of the bottom perturbation for different values of $\hat{r}$. Model parameters are: $\hat{\mu} = 112.5$, $s = 1.02$, $\hat{\Psi}_d = 0.0045$, $\gamma = 0.05$ and $\theta_c = 0.047$.

not change ($\Gamma_r \equiv 0$). When $\hat{r}$ is increased, a critical value $\hat{r}_c$ is found such that the sediment starts to be transported. For $\hat{r}$ slightly larger than $\hat{r}_c$, bottom perturbations, characterized by values of δ falling within a range centred around $\delta_{c,max}$, experience an average amplification within a cycle. An analysis of the results (see figure 5) shows that $\hat{r}_c$ is about 24 and $\delta_{c,max}$ is about 0.07. These values, for a semi-diurnal tide and a water depth equal to 21 m, which is the value measured at SW1, give rise to a critical value of U_m equal to about 0.2 ms^{-1}. A quantitative comparison of present

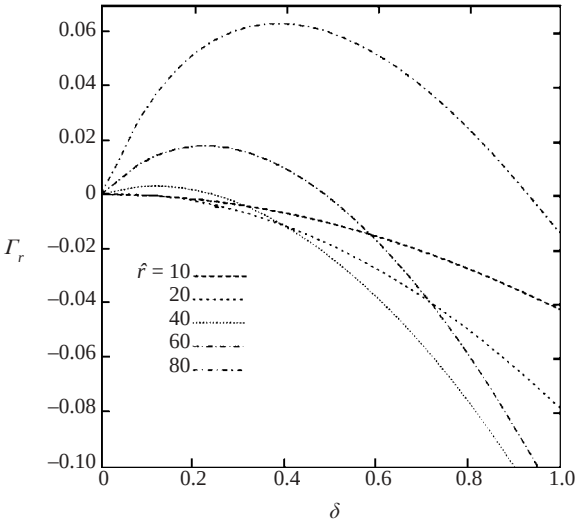

FIGURE 6. As figure 5 except for $\theta_c = 0$.

results with field data is difficult because of the lack of data concerning field critical conditions. Looking at figure 3.2 of Belderson *et al.* (1982), it appears that the critical value of U_m is not too far from the values observed in the field which range around $0.5\,\mathrm{ms}^{-1}$. Incidentally, sand waves have been observed also in sites characterized by weaker tidal currents (at SW1 the semi-diurnal constituent gives rise to a tidal current equal to about $0.4\ \mathrm{ms}^{-1}$). Moreover, close to the critical conditions, the wavelength of the most unstable perturbation (1900 m) is of the same order of magnitude as those observed in the field, even though it turns out to be somewhat larger. The results of figure 5 have been obtained setting $\theta_c = 0.047$. To compare present findings with those obtained by means of sediment transport predictors which neglect the existence of a critical bed shear stress for the erosion of sand, figure 6 shows Γ_r versus δ for different values of $\hat{r}$, the other parameters being equal to those of figure 5 but for $\theta_c = 0$. Even for a vanishing value of θ_c, the model shows the existence of a critical value $\hat{r}_c$ of $\hat{r}$ below which sand waves do not appear. For $\theta_c = 0$, $\hat{r}_c$ turns out to be about 15. For a semi-diurnal tide and a water depth equal to 21 m, this value of $\hat{r}_c$ gives rise to a critical value of U_m equal to about $0.11\ \mathrm{ms}^{-1}$, a value still not far from field observations. On the other hand for $\theta_c = 0$, the wavelength of the most unstable perturbation around the critical conditions tends to infinity. This finding is not better than the results of previous analyses which show that, when the tidal current is strong enough to cause the instability of the flat bottom configuration, ultra-long waves tend to grow (see Komarova & Hulscher 2000 for a detailed discussion). However, realistic values of the parameters lead to values of $\hat{r}$ significantly larger than $\hat{r}_c$ and in this case the most unstable perturbation has a wavelength similar to those observed in the field. Indeed, figure 7, where the dimensionless ratio between the wavelength L_{max} of the most unstable perturbation and the water depth H is plotted versus $\hat{r}$, shows that L_{max}/H rapidly decreases as soon as $\hat{r}$ becomes larger than $\hat{r}_c$ and the wavelength of the most unstable sand waves agrees well with field observations. In figure 7 the results obtained with both $\theta_c = 0.047$ and $\theta_c = 0.0$ are shown.

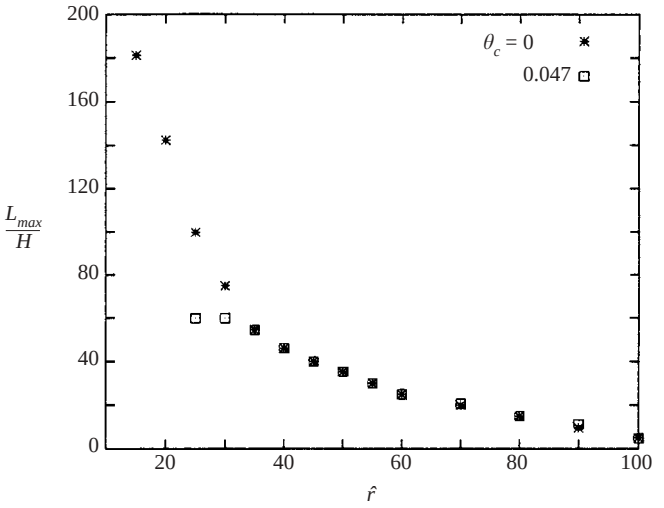

FIGURE 7. Dimensionless ratio between the wavelength L_{max} of the most unstable perturbation and the water depth H *vs.* the parameter $\hat{r}$. Model parameters are: $\hat{\mu} = 112.5$, $s = 1.02$, $\hat{\Psi}_d = 0.0045$ and $\gamma = 0.05$.

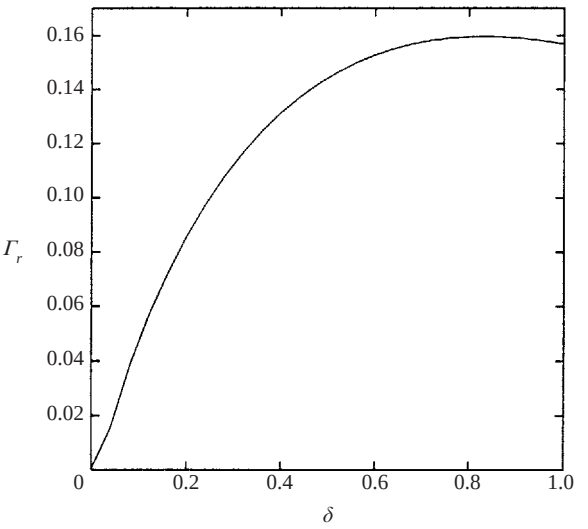

FIGURE 8. Dimensionless growth rate Γ_r *vs.* the dimensionless wavenumber δ of the bottom perturbation. Model parameters are: $\hat{\mu} = 112.5$, $s = 1.50$, $\hat{r} = 79$, $\hat{\Psi}_d = 0.0045$, $\gamma = 0.05$ and $\theta_c = 0.047$.

The results described so far have been obtained assuming that the bottom roughness is due to the presence of medium-size ripples. Sometimes field surveys show that megaripples cover the sea bottom. In this case the bottom roughness is higher and relationships (3.9*a*, *b*) show that the parameter s increases while $\hat{\mu}$ does not change. It is then interesting to look at the amplification rate Γ_r for the same values of the parameters as those of figure 3 but for $s = 1.5$ which is the value of the stress parameter associated to megaripples (see figure 8). The value of δ_{max} turns out to be about 0.8.

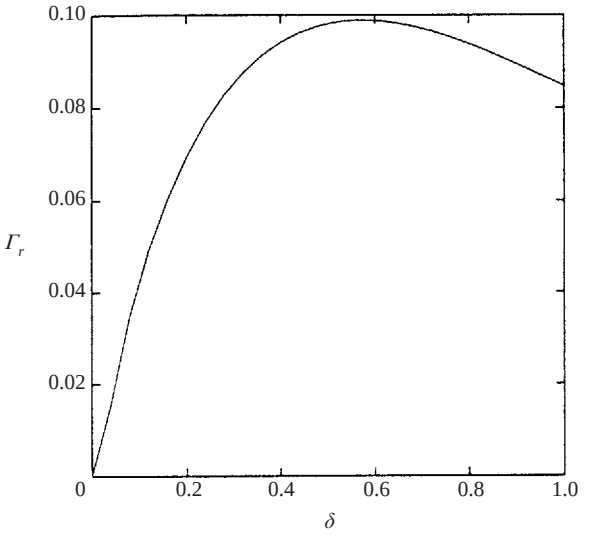

FIGURE 9. As figure 8 except for $\hat{\mu} = 78.1$ and $s = 0.83$.

In this case, at SW1 where $H = 21$ m, the model predicts the appearance of sand waves characterized by a wavelength equal to 160 m. Therefore, considering roughness size ranging from medium-size ripples to megaripples, the predicted wavelength of sand waves falls between 160 m and 315 m, a range which agrees well with field observations.

Looking at the critical conditions, it appears that the value of $\hat{r}_c$ is only slightly affected by s whereas the wavelength of the most unstable perturbation for $\hat{r}$ close to $\hat{r}_c$ significantly decreases if s is increased. For example for $\hat{\mu} = 112.5$, $s = 1.5$, $\hat{\Psi}_d = 0.0045$, $\gamma = 0.05$ and $\theta_c = 0.047$, it turns out that $\hat{r}_c$ is about 24 and δ_{max} is about 0.11.

Similar results have been obtained for different values of the parameters. For example, using a different eddy-viscosity profile (Van Rijn 1991) and assuming the roughness to be induced by medium-size ripples, relationships (3.9a, b) give $\hat{\mu} = 78.12$ and $s = 0.83$. With these values of $\hat{\mu}$ and s and fixing $\hat{r} = 79$, $\hat{\Psi}_d = 0.0045$, $\gamma = 0.05$ and $\theta_c = 0.047$, figure 9 shows that δ_{max} is about 0.55. For $H = 21$ m, this value of δ_{max} gives rise to a wavelength of sand waves equal to about 240 m.

In a particular site, i.e. for a fixed value of H, the conditions leading to the appearance of sand waves have been analysed also keeping fixed the value of $\hat{r}$, i.e. the strength of the tidal current, and considering different values of $\hat{\Psi}_d$, i.e. of the grain size. From the results of figure 10, where Γ_r is plotted versus δ, it appears that decreasing values of $\hat{\Psi}_d$ lead to smaller values of Γ_r until for $\hat{\Psi}_d$ below a critical value $\hat{\Psi}_{dc}$, Γ_r is always negative and sand waves do not appear. Since $\hat{\Psi}_{dc}$ is equal to about 0.0006, for a semi-diurnal tide of amplitude equal to 0.43 ms^{-1} and a water depth equal to 21 m, the critical grain size above which sand waves do not appear is about 1 mm. This finding qualitatively agrees with field observations which show that sand waves develop only in sandy sea beds and they do not appear when a coarse sediment covers the sea bottom. Finally figure 11, where L_{max}/H is plotted versus $\hat{\Psi}_d$, shows that a finer sediment causes the appearance of shorter sand waves. A quantitative comparison between these theoretical findings and field observations is not possible because of the lack of the latter.

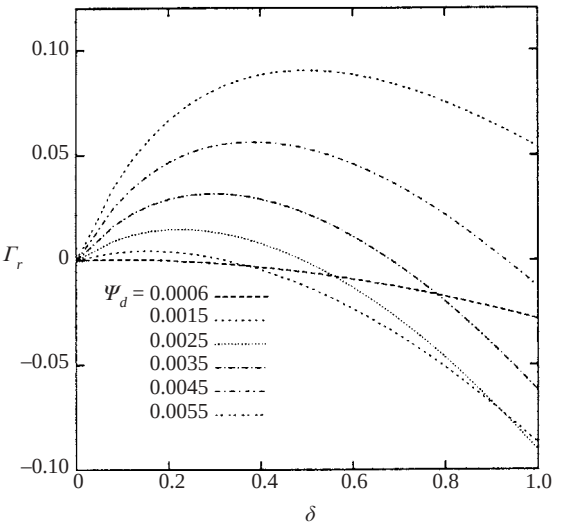

FIGURE 10. Dimensionless growth rate Γ_r plotted versus the dimensionless wavenumber δ of the bottom perturbation for different values of $\hat{\Psi}_d$. Model parameters are: $\hat{\mu} = 112.5$, $s = 1.02$, $\hat{r} = 79$, $\gamma = 0.05$ and $\theta_c = 0.047$.

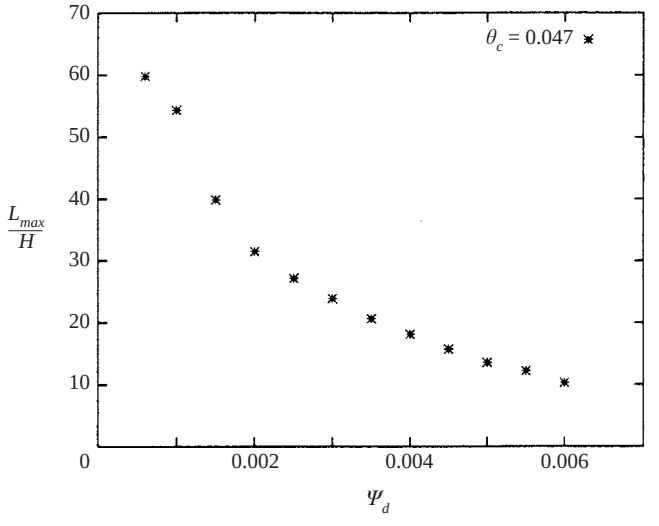

FIGURE 11. Dimensionless ratio between the wavelength of the most unstable perturbation and the water depth H *vs.* the parameter $\hat{\Psi}_d$. Model parameters are: $\hat{\mu} = 112.5$, $s = 1.02$, $\hat{r} = 79$ and $\gamma = 0.05$.

5. Discussion of the model findings

The present analysis supports the idea that sand waves in tide dominated coastal areas arise because of an inherent instability of the flat bottom configuration subject to tidal currents. The mechanism which leads to the growth of sand waves is that suggested by Hulscher (1996*a*): the interaction of an oscillatory tidal current with a bottom waviness gives rise to steady recirculating cells. When the steady streaming close to the bed is directed from the troughs toward the crests of the bottom

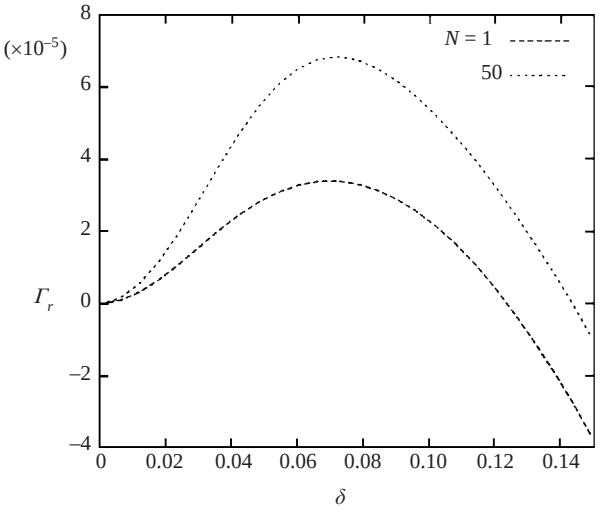

FIGURE 12. Dimensionless growth rate Γ_r *vs.* the dimensionless wavenumber δ of the bottom perturbation for $\hat{\mu} = 112.5$, $s = 1.02$, $\hat{r} = 25$, $\hat{\Psi}_d = 0.0045$, $\gamma = 0.05$, $\theta_c = 0.047$ and $\mathcal{N}$ =1, 50. Larger values of $\mathcal{N}$ provide results coincident with those obtained setting $\mathcal{N} = 50$.

perturbation and is strong enough to overcome gravity effects which tend to carry the sediment from the crests toward the troughs, the perturbation grows and gives rise to bottom patterns.

Present results provides a more accurate description of the phenomenon.

First, the use of a sediment transport formula which takes into account the size of the sediment and the introduction of a critical bed shear stress for sediment motion allows us to predict some aspects of the phenomenon which were not considered by previous models. In fact, according to field observations, the analysis shows that a coarse sediment, even when transported by the tidal current, does not give rise to the appearance of sand waves. Moreover the introduction of a critical shear stress for sediment movement allows a more realistic evaluation of the conditions leading to sand waves appearance and gives rise to a finite value of the wavelength of the most unstable perturbations when the parameters are close to their critical values. However, perturbations characterized by vanishing values of δ are also unstable and ultra-long bed forms grow too. A height- and flow-dependent model for the eddy viscosity has been adopted by Komarova & Hulscher (2000) to resolve the problem of the excitation of these very long sand waves. In the model used by Komarova & Hulscher (2000) and Komarova & Newell (2000), the eddy viscosity changes in time only for a term proportional to the amplitude of the bottom perturbation and becomes time-independent for a flat bottom configuration and the changes of turbulence structure taking place during the tidal cycle are not taken into account. This first attempt of accounting for time variations of the eddy viscosity opens the way to further investigations on the effects of the temporal and spatial structure of turbulence on sand wave formation.

Secondly, the solution procedure holds for arbitrary values of the parameters of the problem. In figure 12, the real part Γ_r of the amplification rate obtained with a large values of $\mathcal{N}$, such that larger values of $\mathcal{N}$ provide results coincident with those displayed in the figure, is plotted versus δ along with its value computed with $\mathcal{N}$ =1, i.e. considering just one harmonic component, for values of the parameters close to

the critical conditions. By looking at the results of figure 12, it appears that values of the parameters exist such that the method of harmonic truncation used by Hulscher (1996*a*) provides a qualitative description of the phenomenon, but it is not accurate from a quantitative point of view. The evaluation of Ψ by means of (3.10) requires large values of $\mathcal{N}$ because the interaction between the oscillatory flow induced by tide propagation and the bottom waviness gives rise to a cascade process which generates many time harmonic components.

For all the results described in the paper, tests have been made to ensure that the results do not depend on the value of $\mathcal{N}$ and cases characterized by realistic values of the parameters can be handled without any problem.

Some aspects of the model can be improved. The actual value of the eddy viscosity, which is introduced to model turbulent stresses, vanishes at the bottom and increases moving far from it, before decreasing near the free surface. Since the model uses a constant eddy viscosity, the well-established no-slip condition at the bottom should be replaced by a partial slip condition. It follows that the model provides a fair description of the flow far from the bottom but it fails to describes the velocity profile close to the sea bed. Moreover, as already pointed out, a time-independent eddy-viscosity model is not accurate at flow reversal. Therefore to have a more accurate description of turbulence, spatial and temporal variations of the eddy viscosity should be taken into account as well as the influence of bottom perturbations on turbulent structure. The sediment transport predictor assumes that sediment moves only as bed load. Rough estimates of the suspended load show that the latter can give a significant contribution to the total load. Moreover the effects of wind waves are not taken into account in the model, although it is known that in shallow seas the oscillatory motion induced by wind waves close to the bottom can pick up sediment which is then transported by the steady currents. Finally, quite often, the local flow induced by tide propagation is not unidirectional and many tide constituents give rise to a complex time development of the actual tidal current.

6. Conclusions

A simple mathematical model capable of reproducing the major features of sand wave inception and growth is described. The present analysis reinforces the idea that sand waves in tide dominated coastal areas arise because of an inherent instability of the flat bottom configuration subject to tidal currents.

Notwithstanding the simplified description of turbulence and sediment transport, the critical conditions for sand wave appearance are fairly estimated and, for realistic values of the parameters, the present results allow the prediction of morphological patterns characterized by wavelengths comparable with those observed in the field.

The present analysis removes some of the limitations of previous works on the subject, even though there is room for further improvements. Moreover being based on a linear approach, the model can predict only the initial stage of bed form growth. In order to investigate the long-term behaviour, when the amplitude of sand waves reach finite values, a nonlinear approach is required.

The authors wish to thank Huib de Swart for comments and suggestions which were used to improve both the analysis and the discussion of the results. P. B. thanks S. J. M. H. Hulscher for a fruitful discussion on some points of the analysis. Thanks are also due to SNAMPROGETTI for funding the research under contract no. 300000848 and providing field data. Further financial support has been

provided by the EU through contract no. EVK3-2000-22014 (HUMOR) and contract no. EVK3-2001-00053 (SANDPIT).

This work is part of the PhD thesis of Giovanni Besio to be submitted in partial fulfilment of his degree.

REFERENCES

Belderson, R. H., Johnson, M. A. & Kenyon, N. H. 1982 *Offshore Tidal Sands. Processes and Deposit* (ed. A. H. Stride), pp. 27–57. Chapman Hall.

Blondeaux, P. 1990 Sand ripples under sea waves. Part 1. Ripple formation. *J. Fluid Mech.* **218**, 1–17.

Blondeaux, P. 2001 Mechanics of coastal forms. *Annu. Rev. Fluid Mech.* **33**, 339–370.

Blondeaux, P. & Vittori, G. 1999 Boundary layer and sediment dynamics under sea waves. *Adv. Coastal Ocean Engng* **4**, 133–190.

Drazin, P. G. & Reid, W. H. 1981 *Hydrodynamic Stability*. Cambridge University Press.

Engelund, F. 1970 Instability of erodible beds. *J. Fluid Mech.* **42**, 225–244.

Fredsøe, J. 1974 On the development of dunes in erodible channels. *J. Fluid Mech.* **64**, 1–16.

Fredsøe, J. 1982 Shape and dimensions of stationary dunes in rivers. *J. Hydraul. Div. ASCE* **108**, (HY8), 932–947.

Fredsøe, J. & Deigaard, R. 1992 *Mechanics of Coastal Sediment Transport*. World Scientific.

Gerkema, T. 2000 A linear stability analysis of tidally generated sand waves. *J. Fluid Mech.* **417**, 303–322.

Hulscher, S. J. M. H. 1996*a* Tidal-induced large-scale regular bed form patterns in a three-dimensional shallow water model. *J. Geophys. Res.* **101** (C9), 20 727–20 744.

Hulscher, S. J. M. H. 1996*b* On validation of a sand waves and sand banks model. *Coastal Engng Conf. 2–6 September, Orlando*, vol. 3, 276, 3574–3587.

Hulscher, S. J. M. H. & van den Brink, G. M. 2001 Comparison between predicted and observed sand waves and sand banks in the North Sea. *J. Geophys. Res.* **106** (C5), 9327–9338.

Hulscher, S. J. M. H., de Swart, H. E. & de Vriend, H. J. 1993 Generation of offshore tidal sand banks and sand waves. *Cont. Shelf Res.* **13**, 1183–1204.

Komarova, N. L. & Hulscher, S. J. M. H. 2000 Linear instability mechanism for sand wave formation. *J. Fluid Mech.* **413**, 219–246.

Komarova, N. L. & Newell, A. C. 2000 Nonlinear dynamics of sand banks and sand waves. *J. Fluid Mech.* **415**, 285–312.

Lin, C. C. 1967 *Theory of Hydrodynamic Stability*. Cambridge University Press.

Meyer-Peter, E. & Müller, R. 1948 Formulas for bedload transport. *III Conf. Intl. Assoc. Hydraul. Res., Stockholm, Sweden.*

Sleath, J. F. A. 1976 On rolling grain ripples. *J. Hydraulic Res.* **14**, 69–81.

Sleath, J. F. A. 1984 *Sea Bed Mechanics* (ed. M. E. McCormick). John Wiley.

de Swart, H. E. & Hulscher, S. J. M. H. 1995 Dynamics of large-scale bed forms in coastal seas. In *Nonlinear Dynamics and Pattern Formation in the Natural Environment* (ed. A. Doelman & A. van Harten), pp. 315–331. Longman.

Van Rijn, L. C. 1991 Sediment transport in combined current and waves. *Proc. Euromech. 262, Sand Transport in Rivers, Estuaries and the Sea* (ed. S. Soulsby & B. Bettes). Balkema.

Vittori, G. 1989 Nonlinear viscous oscillatory flow over a small amplitude wavy wall. *J. Hydraul. Res.* **27**, 267–280.

Vittori, G. & Blondeaux, P. 1990 Sand ripples under sea waves. Part 2. Finite-amplitude development. *J. Fluid Mech.* **218**, 19–39.